

## Supplementary Information

### Nano-sized Ag inserted into ITO films prepared by continuous roll-to-roll sputtering for high-performance, flexible, transparent film heaters

Eun-Hye Ko<sup>a</sup>, Hyo-Joong Kim<sup>a</sup>, Sang-Jin Lee<sup>b</sup>, Jae Heong Lee<sup>b</sup>, and Han-Ki Kim<sup>\*,a</sup>

<sup>a</sup>Kyung Hee University, Department of Advanced Materials Engineering for Information and Electronics, 1 Seocheon, Yongin, Gyeonggi-do 446-701, Republic of Korea

<sup>b</sup>Chemical Materials Solutions Center, Korea Research Institute of Chemical Technology, 141 Gajeongro, Yuseong, Daejeon, 305-600, Republic of Korea

*E-mail:* [imdlhkkim@khu.ac.kr](mailto:imdlhkkim@khu.ac.kr) *Fax:* +82-31-205-2462; *Tel:* ++82-31-201-2462

***Roll-to-roll sputtering process of the ITO/Ag/ITO multilayer:*** Figure S1a shows the pilot-scale RTR sputtering system (Ulvac SPW-060) used to deposit ITO and Ag layers on a flexible PET substrate roll at room temperature. The RTR sputtering system was equipped with a rewind roller, an unwind roller, guiding rollers, main roller, substrate heater and surface treatment system. Using an unwinding and rewinding system, the flexible PET substrate was continuously passed over the ITO and Ag targets. In addition, the tension of the flexible PET substrate was controlled by a load cell in the rolling system. The PET substrate with 700 mm width, 200 m length, and 100  $\mu\text{m}$  thickness was passed over the main roller, which was in mechanical contact with the PET substrates. The rolling speed of the PET substrate could be exactly controlled by the motor speeds of the unwind and rewind rollers. Prior to sputtering, the surface of the PET substrate was pre-heated by substrate passing over 300 °C heater to remove any moisture on the PET substrate. The surface of the PET substrate

was pre-treated with Ar irradiation using a linear ion bombardment system at a DC power of 300 W. After the surface pretreatment, a 40 nm thick bottom ITO layer was sputtered at a constant Ar/O<sub>2</sub> flow ratio of 400/4 sccm, DC power of 2.2 kW, and working pressure of 3 mTorr using dual rectangular ITO targets of 950 × 127 mm<sup>2</sup> geometry placed 100 mm below the main roller. Unlike conventional ITO films sputtered with DC power, a MF power supply was used for ITO sputtering, which is beneficial for growing crystalline ITO films. **Figure S1b** shows a picture of plasma formed on dual ITO targets using MF power.

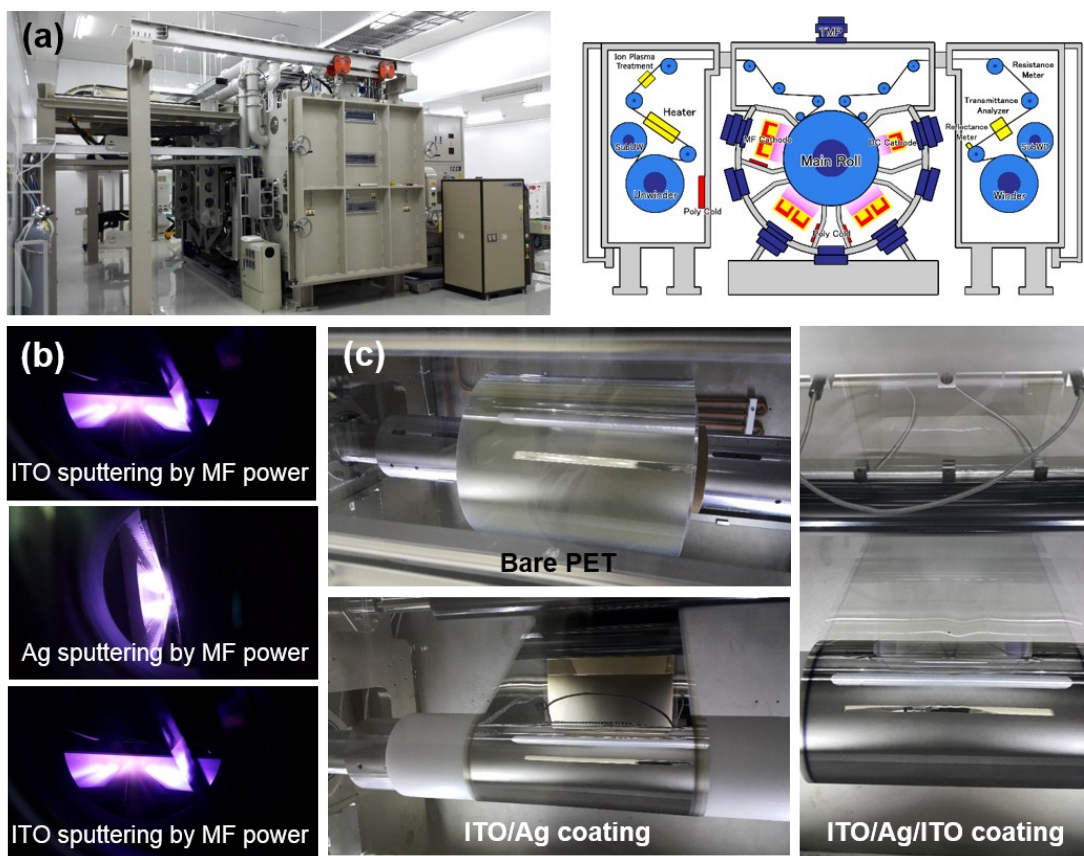


**Figure S1.** (a) Schematic structure and image of pilot-scale RTR sputtering system. (b) Pictures of the plasma formed on dual-ITO targets and the Ag target generated with MF power and DC power respectively. (c) Images of the bare PET substrate before sputtering, the bottom ITO/Ag-coated film, and ITO/Ag/ITO multilayer coated film in the vacuum chamber.

Two cathodes were arrayed with the potential of each cathode periodically changing so the opposite ITO target was as the corresponding anode. The repeated polarity change led to cleaning of the ITO target and reduced probability of arc formation during oxide sputtering. The thickness of the ITO layer was controlled by the MF power applied to dual-ITO targets. After sputtering the bottom ITO layer, an Ag interlayer was then RTR-sputtered onto the bottom ITO layer as a function of thickness at a constant Ar flow of 400 sccm, and working pressure of 3 mTorr, using a rectangular Ag target with  $950 \times 127 \text{ mm}^2$  geometry. The thickness of the Ag interlayer was also controlled by changing the DC power as shown in **Figure S1c**. Finally, a top ITO layer was sputtered onto the Ag interlayer under deposition conditions identical to those used to sputter the bottom ITO layer. The IAI multilayer was sputtered onto the PET substrate in a single chamber using a unwinding and rewinding system without breaking vacuum. **Figure S1c** (Right picture) shows the picture of bare PET, ITO/Ag-coated PET, and ITO/Ag/ITO coated PET in a vacuum chamber, as observed through a glass window on chamber. To investigate the microstructure of the IAI multilayer prepared by RTR sputtering, XRD examination of the IAI sample was performed.

***Fabrication of TFHs with an IAI multilayer:*** To demonstrate the feasibility of the IAI multilayer as a transparent electrode for TFHs, conventional film heaters ( $50 \times 50 \text{ mm}^2$ ) with two-terminal side contact were fabricated on the IAI multilayer electrode as shown in **Figure S2**. For comparison, a-ITO, CNT, graphene, Ag NW, and Ag network films were also used as transparent electrodes. After wet cleaning of the IAI multilayer, a 200 nm-thick Ag side-contact electrode was sputtered onto the IAI multilayer. The DC voltage was supplied to the IAI-based TFHs by a power supply (OPS 3010, ODA technologies) through an Ag contact

electrode at the film edge.

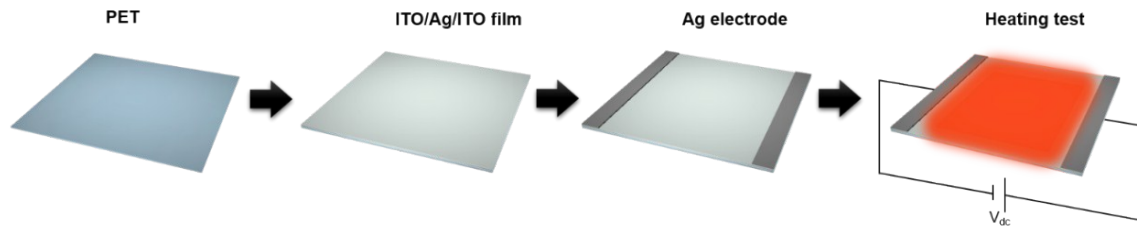


**Figure S2.** Schematic of the TFH fabrication process using RTR-sputtered the IAI multilayer. Two terminal side Ag contact electrodes were fabricated on the IAI multilayer films.

The temperature of the TFHs was measured using a thermocouple mounded on the surface of the TFHs and IR thermal imager (A35sc, FLIR). For the defrost test, the IAI multilayer was placed in a refrigerator for 60 min to form frost on the surface.

**Measurement of the temperature of TFHs:** Figure S3a shows the heating system used to determine the temperature profile of the IAI multilayer-based TFHs. The TFH sample with sputtered Ag side-contact electrodes was fixed between power clips in a black heating system box. The thermocouple was then placed on top of the TFH sample, as shown in Figure 3Sa (Left). DC power was then supplied between the two electrode clips. The temperature of the TFH sample was measured by a thermocouple for a total measurement time of 600 sec (Output mode; On time - 400 sec, Off time - 200 sec). After the temperature profile was obtained, an infrared picture was collected, as shown in Figure S3b, in order to demonstrate the uniformity of the heat distribution over the TFHs. The IR image camera was positioned above the TFH. Finally, the IR image was observed when DC power was supplied by a power supply.

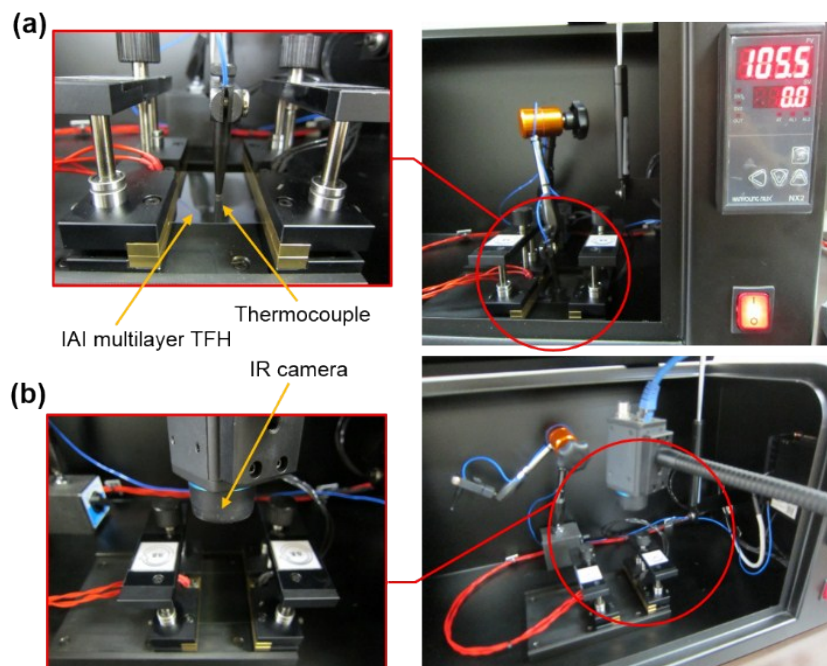


**Figure S3.** Pictures of temperature measurement system for TFH with (a) a thermocouple and (b) IR image camera.

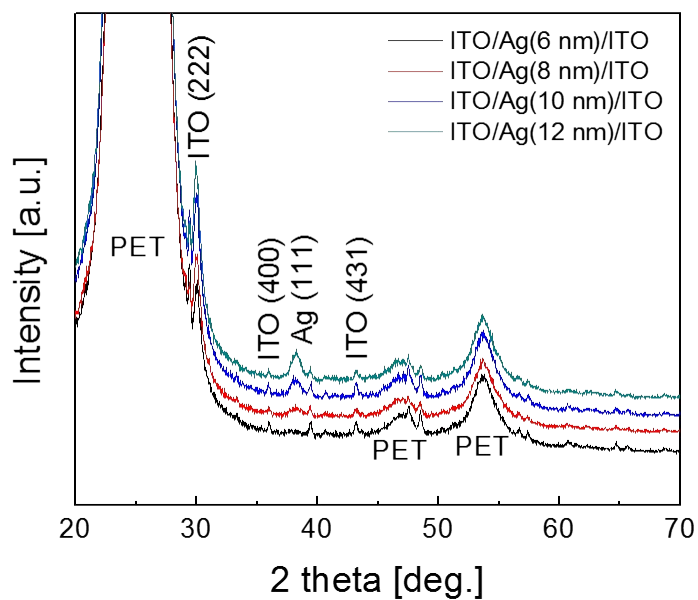


**Figure S4.** XRD plots of the RTR-sputtered IAI multilayer on the PET substrate as a function of Ag thickness.

**Figure S4** showed the XRD plot of the IAI multilayer as a function of Ag thickness. All of the XRD plots of the IAI films show crystalline (222), (400), and (431) peaks at  $2\theta=29.9^\circ$ ,  $36.0^\circ$  and  $43.2^\circ$ , as well as strong PET substrate peaks. The XRD plots of the ITO/Ag/ITO multilayer films showed an additional Ag (111) peak at  $2\theta=38.2^\circ$  with increasing Ag thickness. A clearly distinguished Ag (111) peak was obtained when the Ag layer thickness was greater than 6 nm.